A review, comparison and wake-up call from two deadly Super Typhoons Hato (2017) and Mangkhut (2018)

Zhenzhen Wu[1] and Kelvin T. F. Chan[1]

[1]Sun Yat-sen University

November 22, 2022

Abstract

Super Typhoons Hato (2017) and Mangkhut (2018) have disastrous impacts on the Philippines and South China. Their evolutions and consequences have received wide attention from various media and parties, while the relevant researches are yet limited. Here, we give a full review and comparison of Hato and Mangkhut in terms of their movement, intensity, sizes, and precipitation, targeting to advance the understanding of landfalling super typhoons and to help tropical cyclone forecasting ultimately, especially those over South China. In addition, astoundingly, we reveal that the occurrence of landfalling super typhoons in South China is evidently increasing and tropical cyclones in the northern part of the South China Sea are getting stronger. This study serves as a wake-up call that the threats caused by the tropical cyclones in South China become and may become more catastrophic and frequent in the warming climate.

A review, comparison and wake-up call from two deadly Super Typhoons Hato (2017) and Mangkhut (2018)

Zhenzhen Wu[1,2] and Kelvin T. F. Chan[1,2*]

[1]School of Atmospheric Sciences, and Guangdong Province Key Laboratory for Climate Change and Natural Disaster Studies, Sun Yat-sen University, Zhuhai, China

[2]Southern Marine Science and Engineering Guangdong Laboratory (Zhuhai), Zhuhai, China

*Corresponding author: Kelvin T. F. Chan (chenth25@mail.sysu.edu.cn)

Submitted to
JGR: Atmospheres
January 2020

Key Points:

- Super Typhoons Hato (2017) and Mangkhut (2018) are reviewed and compared
- Tropical cyclones in the northern part of the South China Sea are getting stronger
- Number of landfalling super typhoons in South China is increasing
- Threats caused by the tropical cyclones in South China become and may become more catastrophic and frequent in the warming climate

Abstract

Super Typhoons Hato (2017) and Mangkhut (2018) have disastrous impacts on the Philippines and South China. Their evolutions and consequences have received wide attention from various media and parties, while the relevant researches are yet limited. Here, we give a full review and comparison of Hato and Mangkhut in terms of their movement, intensity, sizes, and precipitation, targeting to advance the understanding of landfalling super typhoons and to help tropical cyclone forecasting ultimately, especially those over South China. In addition, astoundingly, we reveal that the occurrence of landfalling super typhoons in South China is evidently increasing and tropical cyclones in the northern part of the South China Sea are getting stronger. This study serves as a wake-up call that the threats caused by the tropical cyclones in South China become and may become more catastrophic and frequent in the warming climate.

Keywords:

Tropical cyclone; Super typhoon; Hato; Mangkhut; Landfall; Climate change

1 Introduction

Tropical cyclone (TC) is among the most severe natural hazards in the globe which could bring strong winds, heavy rainfall, and storm surges to the proximities. Its consequences can be significant if it is strong, large and/or slow-moving, particularly if it skirts or crosses over the densely populated coastal regions (Zhang et al., 2009; Mori et al., 2014; Hall & Kossin, 2019). South China is known to be one of these, a hot spot where is usually affected by TCs (Liu & Chan, 2003; Chan et al., 2004; Gao et al., 2009; Kuo et al., 2019). Regrettably, it was hit by two deadly Super Typhoons Hato and Mangkhut for two consecutive years in 2017 and 2018, respectively. Their tracks and intensity evolutions are shown in Fig. 1. Hato and Mangkhut brought a series of record-breaking and catastrophic impacts on the Philippines and South China. This study targets to advance the understanding of landfalling super typhoons, like Hato and Mangkhut, by giving a full review and comparison of them.

Hato made landfall in South China and brought severe storm surge to the coast of Pearl River estuary. Sea levels in many areas reached record highs. A maximum storm surge of 2.79 m and a maximum sea level of 6.14 m were recorded at Zhuhai station. Hato brought devastating gales and storm surge to Macao, causing at least 10 deaths and more than 240 injuries and direct economic losses exceeded 8.3 billion MOP. A maximum sea level recorded in A-Ma station was 5.58 m, the highest record in Macao since records began in 1925. The director of the Macao Meteorological and Geophysical Bureau was investigated by the Independent Commission Against Corruption because of the misconduct and dereliction of duty. In the proximities, such as Guangdong, Guangxi, Fujian, Guizhou and Yunnan, at least 15 deaths and 1 missing. About 740000 people were affected, more than 6500 houses collapsed and direct economic losses exceeded 27.2 billion RMB. Due to such ruinous impacts, the name of TC Hato was approved to retire and is replaced by Yamaneko.

Mangkhut brought torrential rain and squalls to Luzon. There were at least 82 deaths, 138 injuries and 2 missing and around 15000 houses collapsed. Also, Mangkhut brought destructive winds and strong storm surge along the coast of South China that caused damages to many buildings and coastal structures. In Macao, around 40 people were injured and more than 5500 people were evacuated. In Inner Harbor of Hong Kong, the height of the inundation once reached 1.9 m or higher above ground. At least 6 people died and more than 3.3 million were affected in Guangdong, Guangxi, Hainan, Guizhou and Yunnan. Like Hato, the name of TC Mangkhut was approved to retire and will be replaced.

Super Typhoons Hato and Mangkhut are investigated in this study because (1) they are the latest two landfalling super typhoons over the South China which still receive limited researches (Takagi et al., 2018; Pun et al., 2019; Zhang et al., 2019); (2) they have comparable tracks over the South China Sea; (3) they made similar landfalls in South China; (4) they brought disastrous impacts on South China; however, (5) they have different evolutions and structural characteristics, for example, movement, intensity, size, and precipitation. Last but not least, (6) Hato and Mangkhut serve as an important wake-up call for us that landfalling super typhoons become and may become more frequent in South China (see last section). Although many studies have been working on TC landfall (Liu & Chan, 2003; Chan et al., 2004), those dedicated to landfalling super typhoons are limited and insufficient (Lee & Bell, 2007; Mori et al., 2014). Hence, this work is critically essential which reviews Super Typhoons Hato and Mangkhut, advances the understanding of landfalling super typhoons, particularly those over the South China, and further suggests a climate outlook that could be insightful for the TC forecasting and climate projection.

2 Data

The best-track data from the Hong Kong Observatory, including TC positions, minimum sea-level pressure and maximum 10-min average winds, of Hato and Mangkhut were adopted. The Joint Typhoon Warning Center (JTWC) best-track data over period 1970–2018 were used for climatic statistics, in which the data in 2018 is provisional. Data starting from 1970 were studied because this can largely avoid the contamination by the data heterogeneities before the introduction of satellite sensing capability about 1970 (Chan, 2019). The hourly fifth generation of European Centre for Medium-Range Weather Forecasts (ECMWF) atmospheric reanalyses of the global climate (ERA5) data were employed to examine the dynamics (e.g., wind, convergence, mid-level mean flow, lower-tropospheric synoptic flow, etc.) and thermodynamics (e.g., water vapor flux, sea surface temperature, surface entropy flux, etc.) associated with the TCs. The hourly Integrated Multi-Satellite Retrievals for Global Precipitation Measurement (GPM) (IMERG) data were used to study the TC precipitation.

3 Movement

Hato is a short-lived TC which formed on 20 August 2017 and dissipated on 24 August (Fig. 1). It formed over the western North Pacific about 740 km east-southeast of Gaoxiong, Taiwan and moved westwards across the Luzon Strait. It then moved northwestward over the South China Sea, made landfall at Macau, China and dissipated. On the other hand, Mangkhut is a long-lived TC which formed on 7 September 2018 and dissipated on 17 September. It formed over the western North Pacific about 2330 km east of Guam, US and moved westwards. It then turned to the northwest about the east of Philippines and made the first landfall across the northern part of Luzon Island of Philippines. It kept moving northwestwards after entering the South China Sea, and then made the second landfall at Jiangmen, China and dissipated.

Hato and Mangkhut are fast-moving storms (Figs. 1 and 2). Hato moved at 24.7 km h^{-1} and Mangkhut moved at 27.6 km h^{-1} on average. The peak movement speeds of Hato and Mangkhut reached about 40 km h^{-1}. Fig. 2 shows that their movement speeds highly correlate to the mid-level mean flows. The mid-level mean flow, so-called steering flow, is estimated by the 400–700 hPa layer wind average within 600-km radius from the TC center. Results therefore suggest that the movement of Hato and Mangkhut are largely driven by the steering flows, particularly the peripheral flows of the strong subtropical high over the western North Pacific (not shown). For example, when Hato and Mangkhut were in the South China Sea, they situated at the southwest side of a strong subtropical high. They were steered by the southeasterly and moved northwestwards.

According to the concept of potential vorticity tendency on TC movement (Chan & Chan, 2016), steering flow is the primary contribution of TC movement, while the asymmetries of diabatic heating and convection are the secondary. The residuals between TC movement speed and mid-level mean flow are therefore largely attributed to the latter. Let's take Mangkhut as an example, the large residuals found between 9–11 September 2018 are largely due to the high asymmetries of diabatic heating and convection (not shown).

4 Intensity

Hato and Mangkhut followed the typical lifecycle, that is, they formed and intensified at first, and then reached peak intensity in the mature stage, weakened after and dissipated at last (Fig. 3). However, their intensification evolutions are untypical. They went through rapid intensification and attained their lifetime peak maximum intensity and minimum sea level pressure at 100 kt and 950 hPa, and 135 kt and 900 hPa, respectively. Rapid intensification is defined as an increase in the maximum winds of a TC of at least 30 kt in a 24-h period. It is approximately the 95th percentile of over-water 24-h intensity changes of Atlantic basin TCs (Kaplan & DeMaria, 2003). The one of Hato took place over the South China Sea on 22 August 2017, while that of Mangkhut took place near Guam over the western North Pacific on 11 September 2018. It is expected that Mangkhut could experience rapid intensification because (1) it moved over the warm pool where the sea surface temperature (SST) was very high (≥29 °C; estimated by the areal average of SST within 200-km radius from the TC center; Fig. 4) which provided a very favorable thermodynamic condition for rapid intensification (Holland, 1997; Chan et al., 2001; Kanada et al., 2017; Li et al., 2019); and (2) it moved quickly such that the associated upwelling effect of subsurface cool water, which is detrimental to TC intensification, is therefore small (Jacob & Shay, 2003; Mei et al., 2012).

Nonetheless, based on the past understanding, the intensity evolution of Hato was not well-expected. Generally, due to the topographic effect, TC tends to maintain and likely weaken when it is about landfall (Tuleya et al., 1984; Bender et al., 1987; Wu, 2001). However, Hato countered. It underwent rapid intensification prior to landfall. There are two possible reasons: (1) it is a fast-moving storm such that the upwelling effect was small; (2) the shallow water over the continental shelf was warm such that even there was upwelling, the upwelling water was still warm enough which could keep providing favorable thermodynamic condition (SST≥29 °C; Fig. 4) for further intensification (Pun et al., 2019).

SST, surface wind and surface humidity can determine the amount of latent heat and sensible heat available to TC from the ocean, and thus, they are all indicative of the potential TC intensity (Emanuel, 1986). Overall, SST underlying Hato and Mangkhut were considerably warm and steady. They ranged 29.3–30.9 °C and 28–29.8 °C, respectively (Fig. 4). Although the relationship between SST and TC intensity is not apparent as there are many other contributing factors which could also affect TC intensity, the relationship between surface heat fluxes and TC intensity is obvious (Fig. 5). Result clearly show that TC intensity highly correlated with surface heat fluxes, in which the latter leads the former a bit. Here, surface heat flux is the areal average of the sum of sensible heat fluxes and latent heat fluxes within 200-km radius from the TC center at the surface. Both Hato and Mangkhut had strong underlying surface heat fluxes. They ranged from 200–450 W m^{-2} and 200–750 W m^{-2}, respectively. Stronger surface heat fluxes found in Mangkhut suggests more heat were extracted from the ocean to the storm, and hence, favoring higher TC intensity. Results also suggest that a TC experiencing surface heat flux of 450 W m^{-2} or above would likely attain Super Typhoon intensity (≥100 kt). In addition, if the thermal energy extracted from the ocean via surface heat flux is much more than what the TC is dynamically consuming, TC would likely undergo rapid intensification soon.

5 Size

Another remarkable structural difference between Hato and Mangkhut is the TC size. Hato is a tiny TC, while Mangkhut is a giant TC. The circulation and convective clouds of Mangkhut are much more extensive than that of Hato (Fig. 6). Due to such large disparity, the azimuthally-averaged radii of fresh-force (11 m s^{-1}; R11) and gale-force (17 m s^{-1}; R17) surface winds from the TC center are used to depict the size of Hato and Mangkhut, respectively (Fig. 7). As the typical horizontal wind structure of a TC is like a Rankine vortex (i.e., winds decrease exponentially with radius from the vortex center), R11 is larger than R17 for a given vortex. Nonetheless, the variations of R11 and R17 largely share the same fashion.

Figure 7 shows that the size of TC generally increases with TC lifetime in open ocean which is consistent with Chan and Chan (2012). It is because the longer time the TC is on the favorable warm water, the more energy could be extracted from the ocean which favors TC intensification and size growth. In addition, the size variations and size growth rates of Hato and Mangkhut are prominent. Due to the topography effect of Taiwan Island and Luzon Island, the size of Hato shrank when it was passing the Luzon Strait (21–22 August 2017). Its circulation was weakened by the friction of high mountains. Hato expanded again after it entered the South China Sea (22–23 August 2017). The prevailing southwesterly water vapor flux channel indicates that the moisture was mainly from the southwesterly Asian summer monsoon (Fig. 8a). Although moistening the TC environment could provide a favorable thermodynamic condition for TC size growth (Hill & Lackmann, 2009), the dynamic condition around Hato, that is the import of angular momentum by environmental synoptic flows (Chan & Chan, 2013), did not coordinate. The band of the southwesterly wind surge was weak and thin, and hence, the size of Hato could not grow much.

On the other hand, the thermodynamic and dynamic conditions in Mangkhut were both favorable for TC size growth. The moisture from the Southern Hemisphere transported by the cross-equatorial flow (Figs. 8b,c) and that from the Bay of Bengal transported by the southwesterly Asian summer monsoon (Fig. 8c) provided a wet environment to Mangkhut. Meanwhile, differing from Hato (i.e., one thin band of southwesterly wind surge), two thick bands of southwesterly wind surges by the cross-equatorial flow (Figs. 8b,c) and the southwesterly Asian summer monsoon (Fig. 8c) are found which imported prominent angular momentum to the vortex. All these favored the size growth of Mangkhut and resulted in a very large TC. Notes that its peak of R17 is about 390 km, which is 150 km larger than the climatology mean size of TCs over the western North Pacific (Chan & Chan, 2012).

In addition, it is noteworthy that Hato and Mangkhut underwent one and two rapid size growths in their lifecycles, respectively (Fig. 7). Rapid size growth is defined as an increase in the size of at least 100 km in a 24-h period. Inspiringly, it is found that all these three rapid size growths share the same condition and mechanism. That is, once the outer-circulation of TC is in contract with or interacts with an environmental wind surge, TC size would grow rapidly via the sudden increment of angular momentum. For example, when Mangkhut encountered the cross-equatorial southwesterly wind surge on about 10 September 2018 (Fig. 8b), it underwent the first rapid size growth (Fig. 7). When it moved to Philippines Sea on about 13 September 2018, it met another southwesterly wind surge from the Asian summer monsoon (Fig. 8c) and underwent the second rapid size growth (Fig. 7). This is indeed an important finding and novelty that can help TC size forecasting and merits further examination.

6 Precipitation

The precipitation of Hato and Mangkhut are also evidently distinct. Figure 9 shows that the precipitation rate of Mangkhut is generally higher than that of Hato which agrees with their intensity. In addition, the precipitation area of Mangkhut is much more extensive than that of Hato (Figs. 9 and 10), which is coherent with their TC sizes. The eyewall of Hato expanded at first but started to contract when it moved to the proximities of Luzon Strait (Fig. 9a). The topographic effects of Taiwan Island and Luzon Island are therefore suggested to be ones of the potential factors leading to such an eyewall contraction. However, there is still no clear explanation for this. Further investigation, especially numerical modelling study, is warranted. Later, the eyewall of Hato kept being small during and after landfall. On the other hand, the eyewall of Mangkhut kept being small and its associating convective clouds were expanding at first up to where it closed to Philippines (Fig. 9b). The eyewall then started to expand during and after landfall in the Luzon Island. Such an eyewall expansion has also been found by Wu et al. (2009) and Chou et al. (2011). Wu et al. (2009) suggested that Luzon Island resulted in the weakening and dissipation of the original eyewall and the early formation of a large outer eyewall by triggering strong outer spiral rainbands offshore. The eyewall then contracted substantially when Mangkhut made landfall in South China, whereas the convective clouds remained widespread.

While TC precipitation has a large axisymmetric component, previous observational (Lonfat et al., 2007; Chen et al., 2006; Cecil, 2007; Ueno, 2007; Xu et al. 2014) and theoretical (Jones, 1995; DeMaria, 1996; Frank & Ritchie, 1999, 2001; Rogers et al., 2003; Ueno, 2008) studies have shown that environmental vertical wind shear leads to an asymmetric component of the vertical motion and precipitation fields. Moreover, some studies (Kimball, 2008; Yu et al., 2015; Chan et al., 2019; Deng et al., 2019) suggest that vertical wind shear can also play a major role in precipitation asymmetry before, during and after landfall. When Hato moved from its cyclogenesis to Luzon Strait, the overall precipitation took place in the southwest quadrant (Fig. 10a). The eyewall expansion can be clearly observed. Later, when it entered the South China Sea (00–12 UTC 22 August 2017), the precipitation maximum remained in the southwest in the outer-core region, whereas the precipitation maximum rotated once cyclonically in the inner core. After Hato made landfall in South China and moved inland, the overall precipitation maximum rotated cyclonically.

Mangkhut also exhibited various precipitation asymmetry features (Fig. 10b). In the early stage (7–10 September 2018), the heaviest precipitation rotated cyclonically from southwest to northeast in the inner core. Later, heavy precipitation concentrated in the southwest, northwest and northeast quadrants on 12 September. On 13 September, precipitation mainly retained in the south. Precipitation was enhanced when Mangkhut was about to made landfall in Luzon Island. Meanwhile, the outer-core rainbands started to keep forming in the southwest and rotated cyclonically to the northeast since 13 September. These are likely related to the interaction between Mangkhut and the Asian summer monsoon. The inner core became relatively dry and eyewall expanded after Mangkhut made landfall in Luzon Island and entered South China Sea. When Mangkhut made second landfall in South China, two precipitation maxima are found in the southwest and northeast quadrants. It is noted that although vertical wind shear can largely explain the prominent precipitation asymmetry such that precipitation maximum likely locates at the downshear or downshear-left side (not shown), it cannot explain the fine phenomena like, a round precipitation rotation in the inner-core region of Hato, persisting rainband generation and rotation of Mangkhut, two precipitation maxima during landfall of Mangkhut, etc. More efforts on the asymmetry of TC precipitation are urged.

7 Wake-up call

In summary, this paper gives a comprehensive review and comparison of two deadly Super Typhoons Hato and Mangkhut. Even though they are both super typhoons, have similar tracks over the South China Sea, and make similar landfalls in South China, their evolutions and structural characteristics, for example, movement, intensity, size, and precipitation, are remarkably different. This study advances the understanding of landfalling super typhoons, especially those over the South China, providing an informative reference for TC forecasting.

Last but not least, astoundingly, this study reveals that the occurrence of landfalling super typhoons in South China is significantly increasing (Fig. 11a). Inclusion of Hato in 2017 and Mangkhut in 2018 substantiates the trend further. It is noteworthy that in the past 49 years (1970–2018), there are totally 11 landfalling super typhoons in South China, in which 6 of them appeared in the last 11 years (2008–2018). The maximum of the annual average of TC intensity in the South China Sea is found to be shifting poleward gradually (Fig. 11b). Although there are some fluctuations from time to time, such poleward shift signal is apparent. This implies that TCs in the northern part of South China Sea are getting stronger, while those in the southern part of South China Sea are getting weaker. In some sense, this finding is in line with the global poleward migration of the location of TC maximum intensity. The poleward migration of the location of TC maximum intensity is significantly linked to the changes in the mean meridional structure of environmental vertical wind shear and potential intensity, and can possibly be linked to tropical expansion (Kossin et al., 2014). The poleward migration is projected to continue under a warming climate (Kossin et al., 2016). Sharmila and Walsh (2018) later suggested that such poleward shift is likely related to the variation of Hadley cell expansion in tropical regions. However, Moon et al. (2015) found that there is an inter-basin variability of the poleward shift. In the Pacific basins, Daloz and Camargo (2018) proposed that the poleward migration of TC maximum intensity should be due to the poleward shift of cyclogenesis. Nonetheless, they did not examine on finer regional scale like South China Sea. The present findings give a profound insight into the local and contingency planning in South China, suggesting that the catastrophic impacts on coastal residents and infrastructure, which threaten life and property, become and may become common.

Under the circumstance of global warming, the situation could be even worse. The warming air allows higher water-vapor capacity of the atmosphere, and thus, will increase in global precipitation and extremes (Allan & Soden, 2008; Kharin et al., 2013; Hegeral et al., 2015; Kitoh & Endo, 2016; Prein et al., 2017). Meanwhile, the warming ocean possesses higher heat potential, and hence, will provide more energy to fuel the TCs. Therefore, the increases in number of intense TCs and the associated precipitation are expected in the warming climate (Knutson et al., 2015; Walsh et al., 2016). Remarkably, Wu et al. (2015) further shows that there is a westward shift of cyclogenesis over the western North Pacific. The landfalling super typhoons in South China may become more frequent. What's more, the sea level rise due to global warming will raise the frequency and threat of severe storm surge along the coast.

Super Typhoons Hato and Mangkhut give us a wake-up call that we must not underrate the power of nature and the challenges of climate change. We must stay alert and be well prepared to confront the even higher threats of TCs and extreme weather in the future. Notes that the finding and discussion presented here do not constitute a detection and attribution study. Further study of the increase in the occurrence of landfalling super typhoons in South China, and the potential link to the observed tropical expansion, which is thought to have global warming contributions, is warranted.

Acknowledgments

We sincerely thank the Hong Kong Observatory for providing the summary of the devastation and casualty reports, best-track data, and satellite imageries. This study was supported by the National Natural Science Foundation of China (41975052), the National Natural Science Foundation of China and Macau Science and Technology Development Joint Fund (NSFC-FDCT), China and Macau (41861164027) and the Fundamental Research Funds for the Central Universities (74110-31610017).

Data availability

The JTWC best-track data was taken from https://www.ncdc.noaa.gov/ibtracs/. The HKO best-track data was requested from HKO. The ERA5 reanalysis data were downloaded from https://www.ecmwf.int/en/forecasts/datasets/reanalysis-datasets/era5. The IMERG precipitation data was retrieved from https://www.nasa.gov/mission_pages/GPM/main/index.html.

Author contributions

ZW conducted the analyses. KTFC supervised the study. ZW and KTFC contributed to the discussion of the results and writing of the paper.

Declaration of Competing Interest

The authors declare that they have no conflict of interests.

References

Allan, R. P., & Soden, B. J. (2008). Atmospheric warming and the amplification of precipitation extremes. *Science*, *321*(5895), 1481–1484. https://doi.org/10.1126/science.1160787

Bender, M. A., Tuleya, R. E., & Kurihara, Y. (1987). A numerical study of the effect of island terrain on tropical cyclones. *Monthly Weather Review*, *115*(1), 130–155. https://doi.org/10.1175/1520-0493(1987)115<0130:ANSOTE>2.0.CO;2

Cecil, D. J. (2007). Satellite-derived rain rates in vertically sheared tropical cyclones. *Geophysical Research Letters*, *34*(2), L02811. https://doi.org/10.1029/2006GL027942

Chan, J. C. L., Duan, Y., & Shay, L. K. (2001). Tropical cyclone intensity change from a simple ocean-atmosphere coupled model. *Journal of the Atmospheric Sciences*, *58*(2), 154–172. https://doi.org/10.1175/1520-0469(2001)058<0154:TCICFA>2.0.CO;2

Chan, J. C. L., Liu, K. S., Ching, S. E., & Lai, E. S. (2004). Asymmetric distribution of convection associated with tropical cyclones making landfall along the South China coast. *Monthly Weather Review*, *132*(10), 2410–2420. https://doi.org/10.1175/1520-0493(2004)132<2410:ADOCAW>2.0.CO;2

Chan, K. T. F. (2019). Are global tropical cyclones slowing down in a warming climate? *Environmental Research Letters*. https://doi.org/10.1088/1748-9326/ab4031 (in press)

Chan, K. T. F., & Chan, J. C. L. (2012). Size and strength of tropical cyclones as inferred from QuikSCAT data. *Monthly Weather Review*, *140*(3), 811–824. https://doi.org/10.1175/MWR-D-10-05062.1

Chan, K. T. F., & Chan, J. C. L. (2013). Angular momentum transports and synoptic flow patterns associated with tropical cyclone size change. *Monthly Weather Review*, *141*(11), 3985–4007. https://doi.org/10.1175/MWR-D-12-00204.1

Chan, K. T. F., & Chan, J. C. L. (2016). Tropical cyclone recurvature: An intrinsic property? *Geophysical Research Letters*, *43*(16), 8769–8774. https://doi.org/10.1002/2016GL070352

Chan, K. T. F., Chan, J. C. L., & Wong, W. K. (2019). Rainfall asymmetries of landfalling tropical cyclones along the South China coast. *Meteorological Applications*, *26*(2), 213–220. https://doi.org/10.1002/met.1754

Chen, S. S., Knaff, J. A., & Marks Jr., F. D. (2006). Effects of vertical wind shear and storm motion on tropical cyclone rainfall asymmetries deduced from TRMM. *Monthly Weather Review*, *134*(11), 3190–3208. https://doi.org/10.1175/MWR3245.1

Chou, K. H., Wu, C. C., & Wang, Y. (2011). Eyewall evolution of typhoons crossing the Philippines and Taiwan: an observational study. *Terrestrial, Atmospheric & Oceanic Sciences*, *22*(6), 535–548. https://doi.org/10.3319/TAO.2011.05.10.01(TM)

Daloz, A. S., & Camargo, S. J. (2018). Is the poleward migration of tropical cyclone maximum intensity associated with a poleward migration of tropical cyclone genesis? *Climate Dynamics*, *50*(1-2), 705–715. https://doi.org/10.1007/s00382-017-3636-7

DeMaria, M. (1996). The effect of vertical shear on tropical cyclone intensity change. *Journal of the Atmospheric Sciences*, *53*(14), 2076–2088. https://doi.org/10.1175/1520-0469(1996)053<2076:TEOVSO>2.0.CO;2

Deng, L., Gao, W., & Duan, Y. (2019). A modeling study of the effects of vertical wind shear on the raindrop size distribution in Typhoon Nida (2016). *Journal of Geophysical Research: Atmospheres*, *124*(12), 6501–6517. https://doi.org/10.1029/2018JD029946

Emanuel, K. A. (1986). An air-sea interaction for tropical cyclones. Part I: Steady-state maintenance. *Journal of the Atmospheric Sciences*, *43*(6), 585–604. https://doi.org/10.1175/1520-0469(1986)043<0585:AASITF>2.0.CO;2

Frank, W. M., & Ritchie, E. A. (1999). Effects of environmental flow upon tropical cyclone structure. *Monthly Weather Review*, *127*(9), 2044–2061. https://doi.org/10.1175/1520-0493(1999)127<2044:EOEFUT>2.0.CO;2

Frank, W. M., & Ritchie, E. A. (2001). Effects of vertical wind shear on the intensity and structure of numerically simulated hurricanes. *Monthly Weather Review*, *129*(9), 2249–2269. https://doi.org/10.1175/1520-0493(2001)129<2249:EOVWSO>2.0.CO;2

Gao, S., Meng, Z., Zhang, F., & Bosart, L. F. (2009). Observational analysis of heavy rainfall mechanisms associated with severe Tropical Storm Bilis (2006) after its landfall. *Monthly Weather Review*, *137*(6), 1881–1897. https://doi.org/10.1175/2008MWR2669.1

Hall, T. M., & Kossin, J. P. (2019). Hurricane stalling along the North American coast and implications for rainfall. *Climate and Atmospheric Science*, *2*(1), 17. https://doi.org/10.1038/s41612-019-0074-8

Hegerl, G. C., Black, E., Allan, R. P., Ingram, W. J., Polson, D., Trenberth, K. E., Chadwick, R. S., Arkin, P. A., Sarojini, B. B., Becker, A., Dai, A., Durack, P. J., Easterling, D., Fowler, H. J., Kendon, E. J., Huffman, G. J., Liu, C., Marsh, R., New, M., Osborn, T. J., Skliris, N., Stott, P. A., Vidale, P. L., Wijffels, S. E., Wilcox, L. J., Willett, K. M., & Zhang, X. (2015).

Challenges in quantifying changes in the global water cycle. *Bulletin of the American Meteorological Society*, *100*(10), 1097–1115. https://doi.org/10.1175/BAMS-D-13-00212.1

Holland, G. J. (1997). The maximum potential intensity of tropical cyclones. *Journal of the Atmospheric Sciences*, *54*(21), 2519–2541. https://doi.org/10.1175/1520-0469(1997)054<2519:TMPIOT>2.0.CO;2

Jacob, S. D., & Shay, L. K. (2003). The role of oceanic mesoscale features on the tropical cyclone-induced mixed layer response: A case study. *Journal of Physical Oceanography*, *33*(4), 649–676. https://doi.org/10.1175/1520-0485(2003)33<649:TROOMF>2.0.CO;2

Hill, K. A., & Lackmann, G. M. (2009). Influence of environmental humidity on tropical cyclone size. *Monthly Weather Review*, *137*(10), 3294–3315. https://doi.org/10.1175/2009MWR2679.1

Jones, S. C. (1995). The evolution of vortices in vertical shear: I: Initially barotropic vortices. *Quarterly Journal of the Royal Meteorological Society*, *121*(524), 821–851. https://doi.org/10.1002/qj.49712152406

Kaplan J., & DeMaria, M. (2003). Large-scale characteristics of rapidly intensifying tropical cyclones in the North Atlantic basin. *Weather and Forecasting*, *18*(6), 1093–1108. https://doi.org/10.1175/1520-0434(2003)018<1093:LCORIT>2.0.CO;2

Kanada, S., Tsujino, S., Aiki, H., Yoshioka, M. K., Miyazawa, Y., Tsuboki, K., & Takayabu, I. (2017). Impacts of SST patterns on rapid intensification of Typhoon Megi (2010). *Journal of Geophysical Research: Atmospheres*, *122*(24), 245–262. https://doi.org/10.1002/2017JD027252

Kharin, V. V., Zwiers, F. W., Zhang, X., & Wehner, M. (2013). Changes in temperature and precipitation extremes in the CMIP5 ensemble. *Climatic Change*, *119*(2), 345–357. https://doi.org/10.1007/s10584-013-0705-8

Kimball, S. K. (2008). Structure and evolution of rainfall in numerically simulated landfalling hurricanes. *Monthly Weather Review*, *136*(10), 3822–3847. https://doi.org/10.1175/2008MWR2304.1

Kitoh, A., & Endo, H. (2016). Changes in precipitation extremes projected by a 20-km mesh global atmospheric model. *Weather Climate Extremes*, *11*, 41–52. https://doi.org/10.1016/j.wace.2015.09.001

Knutson, T. R., Sirutis, J. J., Zhao, M., Tuleya, R. E., Bender, M., Vecchi, G. A., Villarini, G., & Chavas, D. (2015). Global projections of intense tropical cyclone activity for the late twenty-first century from dynamical downscaling of CMIP5/RCP4.5 scenarios. *Journal of Climate*, *28*(18), 7203–7224. https://doi.org/10.1175/JCLI-D-15-0129.1

Kossin, J. P., Emanuel, K. A., & Vecchi, G. A. (2014). The poleward migration of the location of tropical cyclone maximum intensity. *Nature*, *509*, 349. https://doi.org/10.1038/nature13278

Kossin, J. P., Emanuel, K. A., & Camargo, S. J. (2016). Past and projected changes in western North Pacific tropical cyclone exposure. *Journal of Climate*, *29*(16), 5725–5739. https://doi.org/10.1175/JCLI-D-16-0076.1

Kuo, H. C., Tsujino, S., Huang, C. C., Wang, C. C., & Tsuboki, K. (2019). Diagnosis of the Dynamic Efficiency of Latent Heat Release and the Rapid Intensification of Supertyphoon Haiyan (2013). *Monthly Weather Review*, *147*(4), 1127–1147. https://doi.org/10.1175/MWR-D-18-0149.1

Lee, W. C., & Bell, M. M. (2007). Rapid intensification, eyewall contraction, and breakdown of Hurricane Charley (2004) near landfall. *Geophysical Research Letters*, *34*(2), L02802. https://doi.org/10.1029/2006GL027889

Li, M. X., Ping, F., Tang, X. B., & Yang, S. (2019). Effects of microphysical processes on the rapid intensification of Super-Typhoon Meranti. *Atmospheric Research*, *219*, 77–94. https://doi.org/10.1016/j.atmosres.2018.12.031

Liu, K. S., & Chan, J. C. L. (2003). Climatological characteristics and seasonal forecasting of tropical cyclones making landfall along the South China coast. *Monthly Weather Review*, *131*(8), 1650–1662. https://doi.org/10.1175//2554.1

Lonfat, M., Rogers, R., Marchok, T., & Marks Jr., F. D. (2007). A parametric model for predicting hurricane rainfall. *Monthly Weather Review*, *135*(9), 3086–3097. https://doi.org/10.1175/MWR3433.1

Mei, W., Pasquero, C., & Primeau, F. (2012). The effect of translation speed upon the intensity of tropical cyclones over the tropical ocean. *Geophysical Research Letters*, *39*(7), L07801. https://doi.org/10.1029/2011GL050765

Moon, I. J., Kim, S. H., Klotzbach, P., & Chan, J. C. L. (2015). Roles of interbasin frequency changes in the poleward shifts of the maximum intensity location of tropical cyclones. *Environmental Research Letters*, *10*(10), 104004. https://doi.org/10.1088/1748-9326/10/10/104004

Mori, N., Kato, M., Kim, S., Mase, H., Shibutani, Y., Takemi, T., Tsuboki, K., & Yasuda, T. (2014). Local amplification of storm surge by Super Typhoon Haiyan in Leyte Gulf. *Geophysical Research Letters*, *41*(14), 5106–5113. https://doi.org/10.1002/2014GL060689

Prein, A. F., Rasmussen, R. M., Ikeda, K., Liu, C., Clark, M. P., & Holland, G. J. (2017). The future intensification of hourly precipitation extremes. *Nature Climate Change*, *7*(1), 48–52. https://doi.org/10.1038/nclimate3168

Pun, I. F., Chan, J. C. L., Lin, I. I., Chan, K. T. F., Price, J. F., Ko, D. S., Lien, C. C., Wu, Y. L., & Huang, H. C. (2019). Rapid intensification of Typhoon Hato (2017) over shallow water. *Sustainability*, *11*(13), 3709. https://doi.org/10.3390/su11133709

Rogers, R., Chen, S., Tenerelli, J., & Willoughby, H. (2003). A numerical study of the impact of vertical shear on the distribution of rainfall in Hurricane Bonnie (1998). *Monthly Weather Review*, *131*(8), 1577–1599. https://doi.org/10.1175//2546.1

Sharmila, S., & Walsh, K. J. E. (2018). Recent poleward shift of tropical cyclone formation linked to Hadley cell expansion. *Nature Climate Change*, *8*(8), 730–736. https://xs.scihub.ltd/https://doi.org/10.1038/s41558-018-0227-5

Takagi, H., Xiong, Y., & Furukawa, F. (2018). Track analysis and storm surge investigation of 2017 Typhoon Hato: were the warning signals issued in Macau and Hong Kong timed appropriately? *Georisk: Assessment and Management of Risk for Engineered Systems and Geohazards*, *12*(4), 297–307. https://doi.org/10.1080/17499518.2018.1465573

Tuleya, R. E., Bender, M. A., & Kurihara, Y. (1984). A simulation study of the landfall of tropical cyclones. *Monthly Weather Review*, *112*(1), 124–136. https://doi.org/10.1175/1520-0493(1984)112<0124:ASSOTL>2.0.CO;2

Ueno, M. (2007). Observational analysis and numerical evaluation of the effects of vertical wind shear on the rainfall asymmetry in the typhoon inner-core region. *Journal of the Meteorological Society of Japan*, *85*(2), 115–136. https://doi.org/10.2151/jmsj.85.115

Ueno, M. (2008). Effects of vertical wind shear on the inner-core asymmetries and vertical tilt of a simulated tropical cyclone. *Journal of the Meteorological Society of Japan*, *86*(4), 531–555. https://doi.org/10.2151/jmsj.86.531

Walsh, K. J. E., McBride, J. L., Klotzbach, P. J., Balachandran, S., Camargo, S. J., Holland, G., Knutson, T. R., Kossin, J. P., Lee, T. C., Sobel, A., & Sugi, M. (2016). Tropical cyclones and climate change. *Wiley Interdisciplinary Reviews: Climate Change*, *7*(1), 65–89. https://doi.org/10.1002/wcc.371

Wu, C. C. (2001). Numerical simulation of Typhoon Gladys (1994) and its interaction with Taiwan terrain using the GFDL hurricane model. *Monthly Weather Review*, *129*(6), 1533–1549. https://doi.org/10.1175/1520-0493(2001)129<1533:NSOTGA>2.0.CO;2

Wu, C. C., Cheng, H. J., Wang, Y., & Chou, K. H. (2009). A numerical investigation of the eyewall evolution in a landfalling typhoon. *Monthly Weather Review*, *137*(1), 21–40. https://doi.org/10.1175/2008MWR2516.1

Wu, L. G., Wang, C., & Wang, B. (2015). Westward shift of western North Pacific tropical cyclogenesis. *Geophysical Research Letters*, *42*(5), 1537–1542. https://doi.org/10.1002/2015GL063450

Xu, W. X., Jiang, H. Y., & Kang, X. B. (2014). Rainfall asymmetries of tropical cyclones prior to, during, and after making landfall in South China and Southeast United States. *Atmospheric Research*, *139*, 18–26. https://doi.org/10.1016/j.atmosres.2013.12.015

Yu, Z., Wang, Y., & Xu, H. (2015). Observed rainfall asymmetry in tropical cyclones making landfall over China. *Journal of Applied Meteorology and Climatology*, *54*(1), 117–136. https://doi.org/10.1175/JAMC-D-13-0359.1

Zhang, Q., Wu, L., & Liu, Q. (2009). Tropical cyclone damages in China 1983–2006. *Bulletin of the American Meteorological Society*, *90*(4), 489–496. https://doi.org/10.1175/2008BAMS2631.1

Zhang, Z., Wang, Y., Zhang, W., & Xu, J. (2019). Coastal ocean response and its feedback to Typhoon Hato (2017) over the South China Sea: A numerical study. *Journal of Geophysical Research: Atmospheres*. https://doi.org/10.1029/2019JD031377

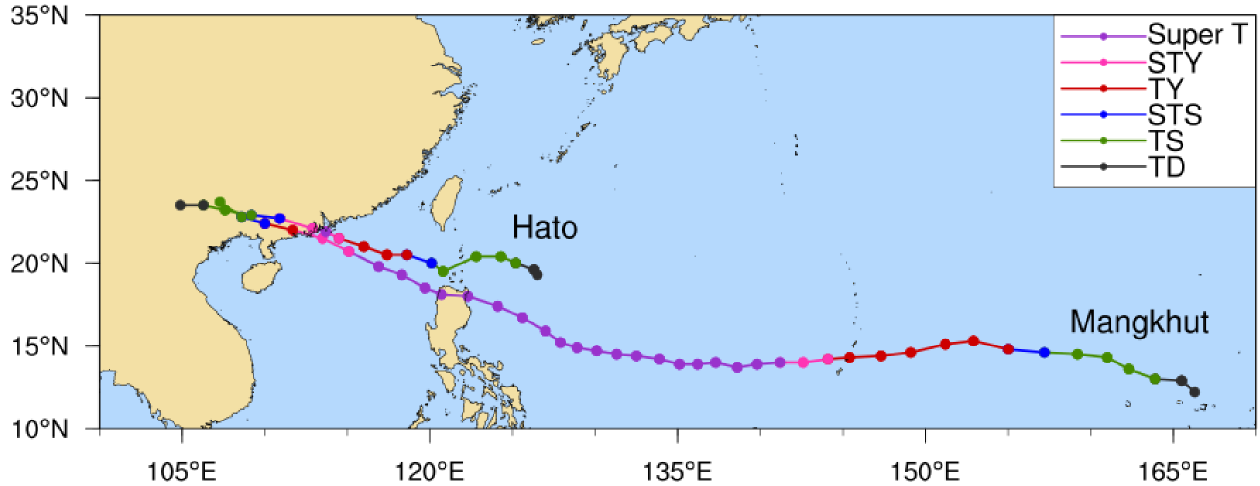

Figure 1. Best tracks and intensity evolutions (TD, tropical depression; TS, tropical storm; STS, severe tropical storm; TY, typhoon; STY, severe typhoon; Super T, super typhoon) of Hato (from 12 UTC 20 Aug to 12 UTC 24 Aug 2017) and Mangkhut (from 06 UTC 7 Sep to 06 UTC 17 Sep 2018). Track markers are all in six-hourly interval, except the one of Hato at Macau is in the middle of the neighbors.

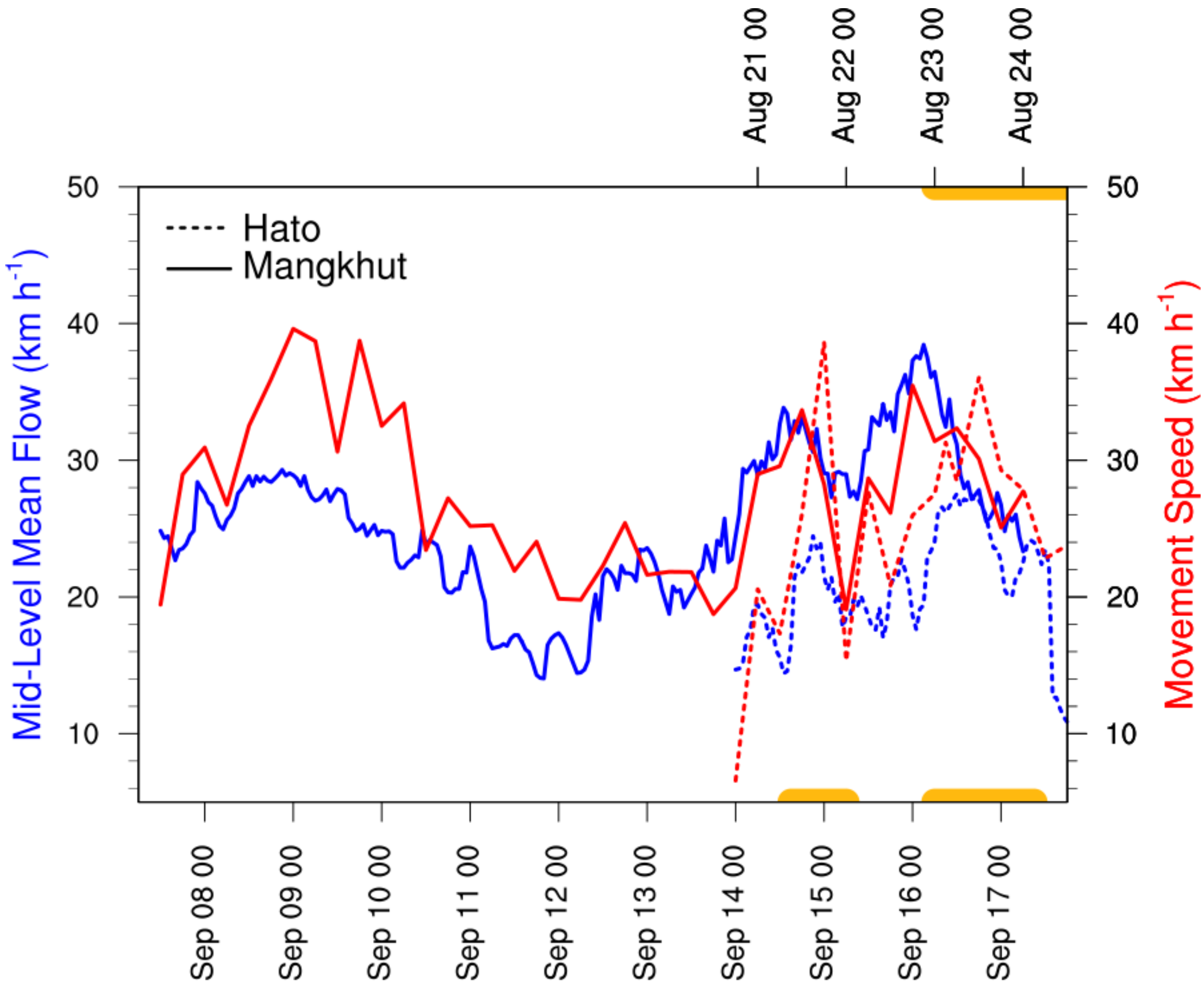

Figure 2. Movement speeds and mid-level mean flows of Hato and Mangkhut. Top and bottom x-axes indicate the lifecycles of Hato and Mangkhut, respectively. The goldenrod bars on the x-axes denote the periods when TCs were over land. For example, the first and second bars on the bottom x-axis depict the periods that Mangkhut was crossing the Philippine and made landfall in the South China, respectively.

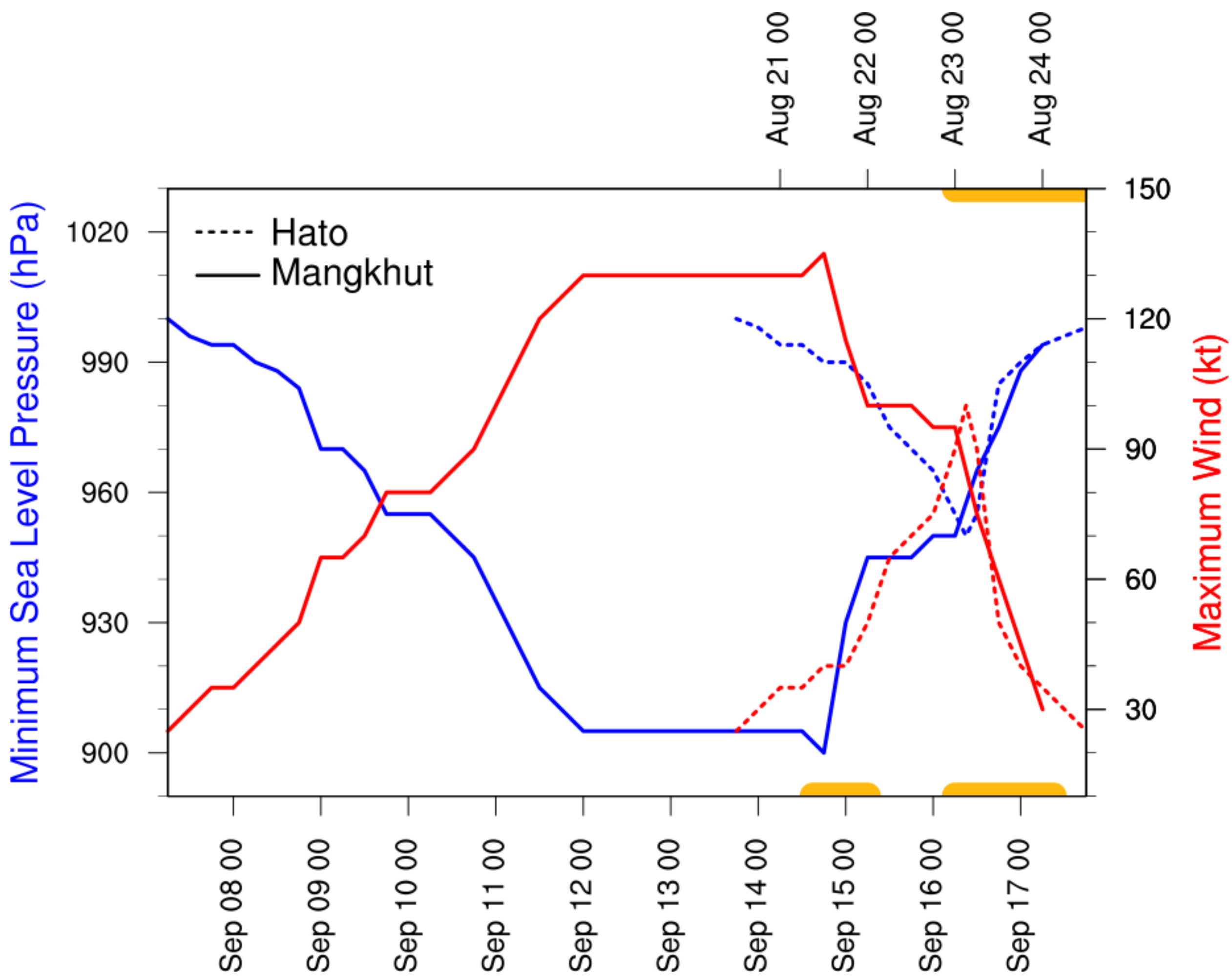

Figure 3. As in Fig. 2, but for minimum sea level pressure and maximum winds of Hato and Mangkhut.

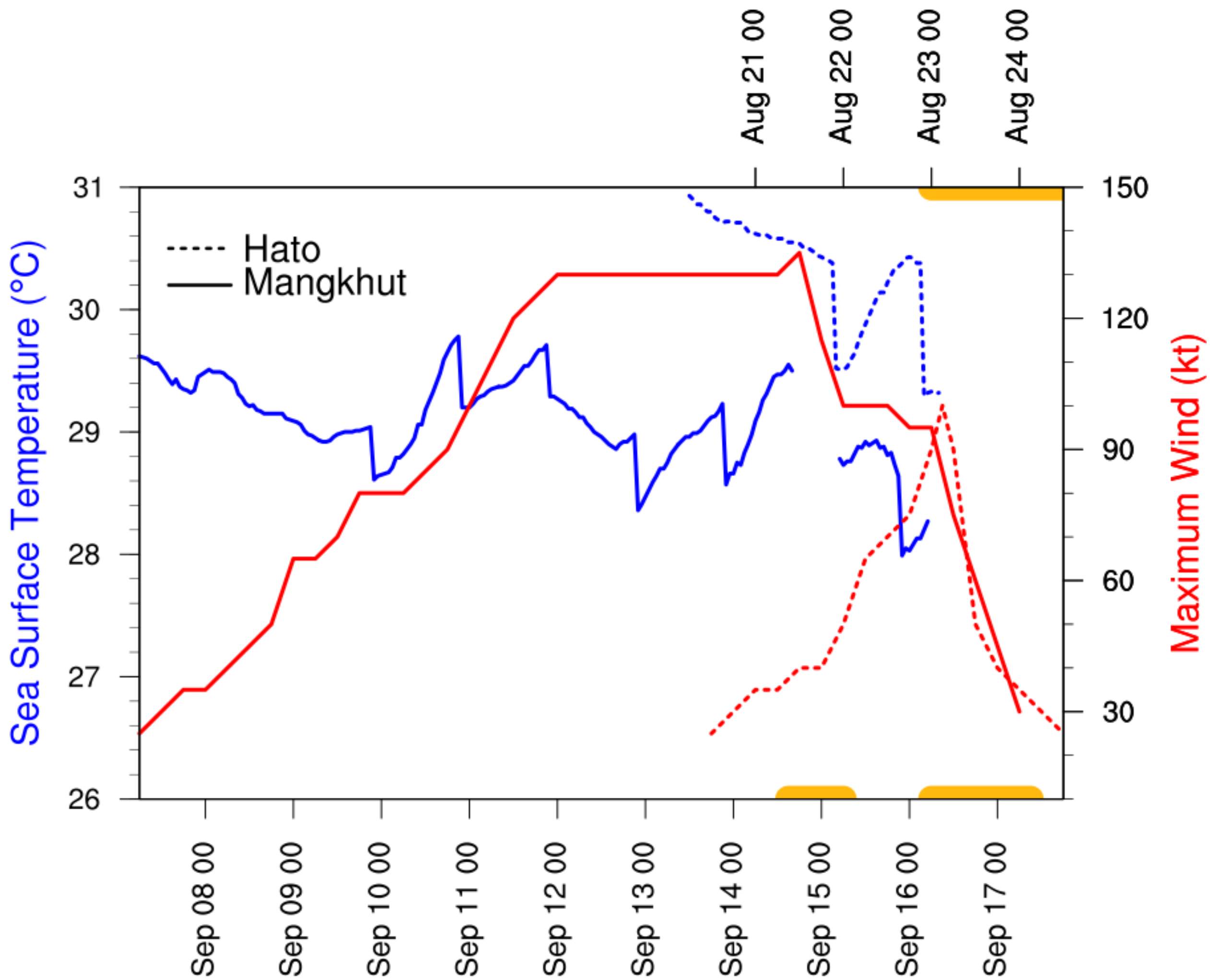

Figure 4. As in Fig. 2, but for sea surface temperature and maximum winds of Hato and Mangkhut. No sea surface temperature data is over land.

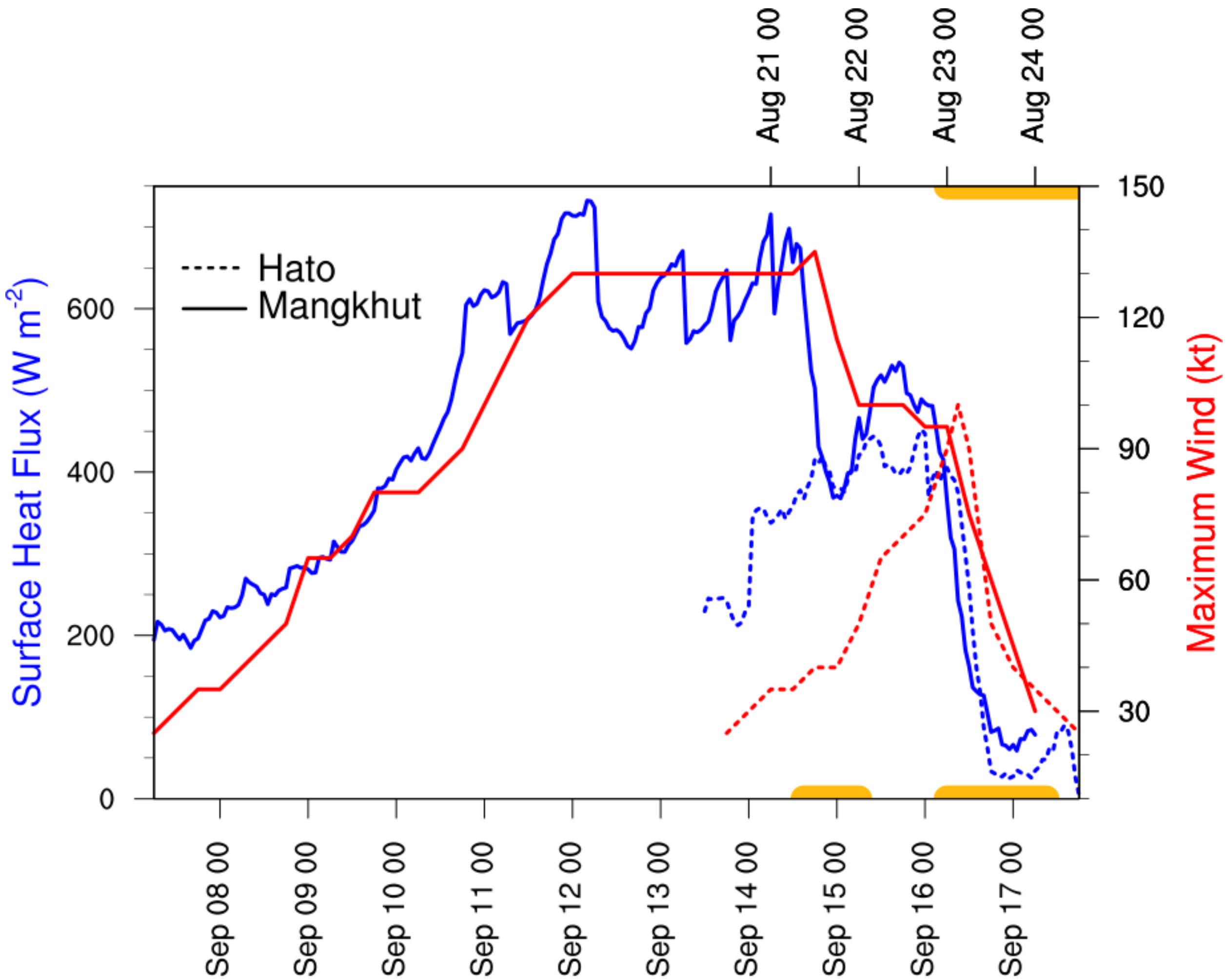

Figure 5. As in Fig. 2, but for the surface heat flux and maximum of winds of Hato and Mangkhut.

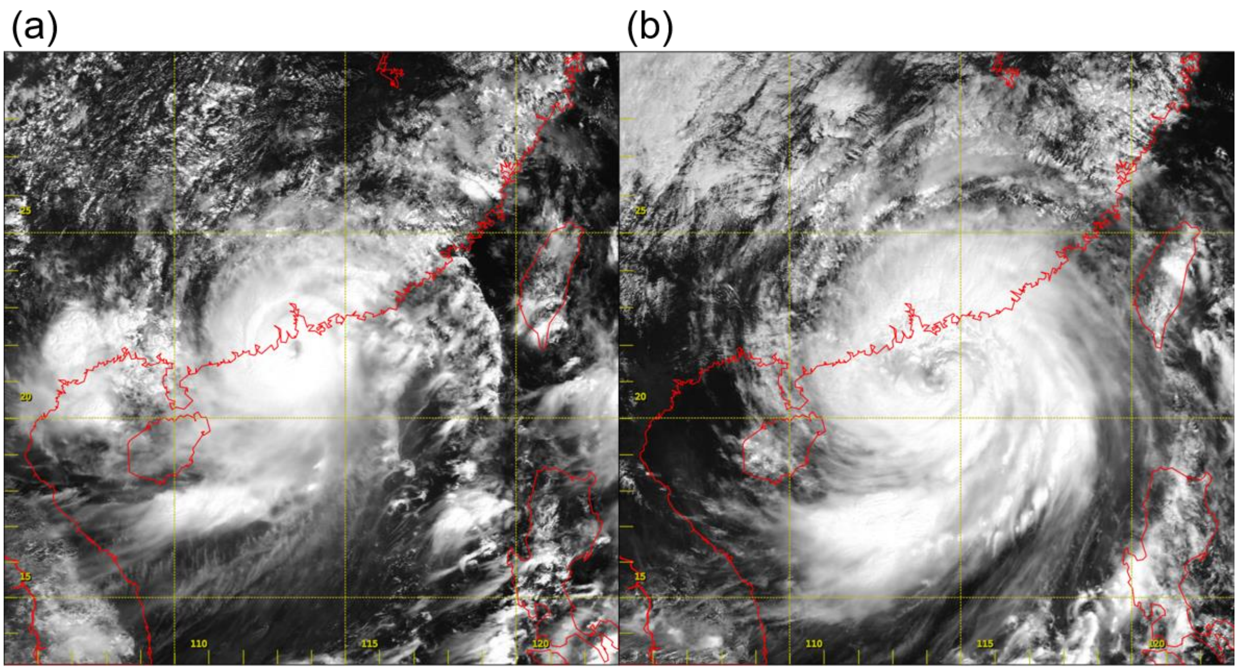

Figure. 6. Visible satellite imageries of Hato at 03 UTC on 23 August 2017 and Mangkhut at 03 UTC on 16 September 2018. Both imageries are on the same scale.

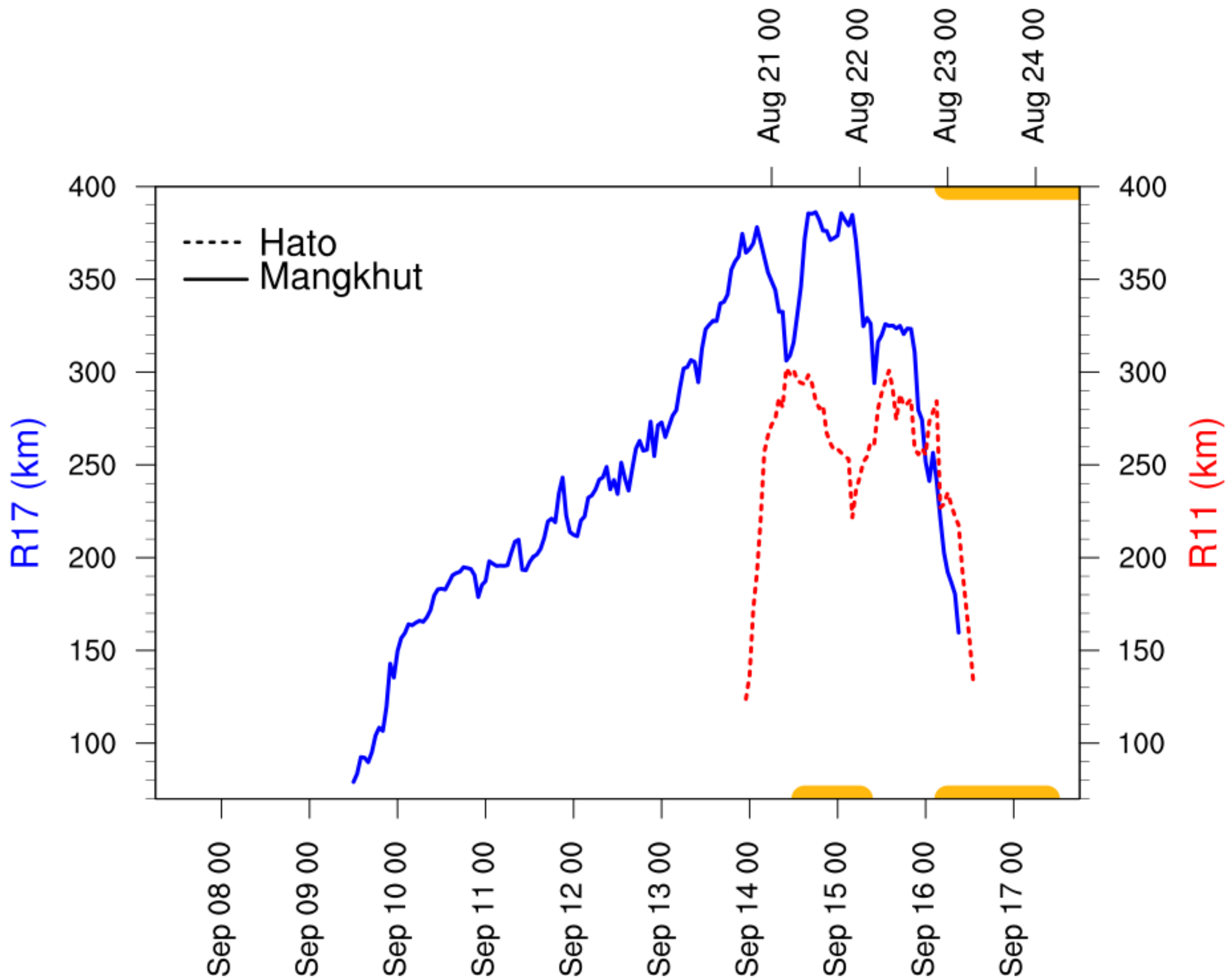

Figure 7. As in Fig. 2, but for R11 and R17 of Hato and Mangkhut.

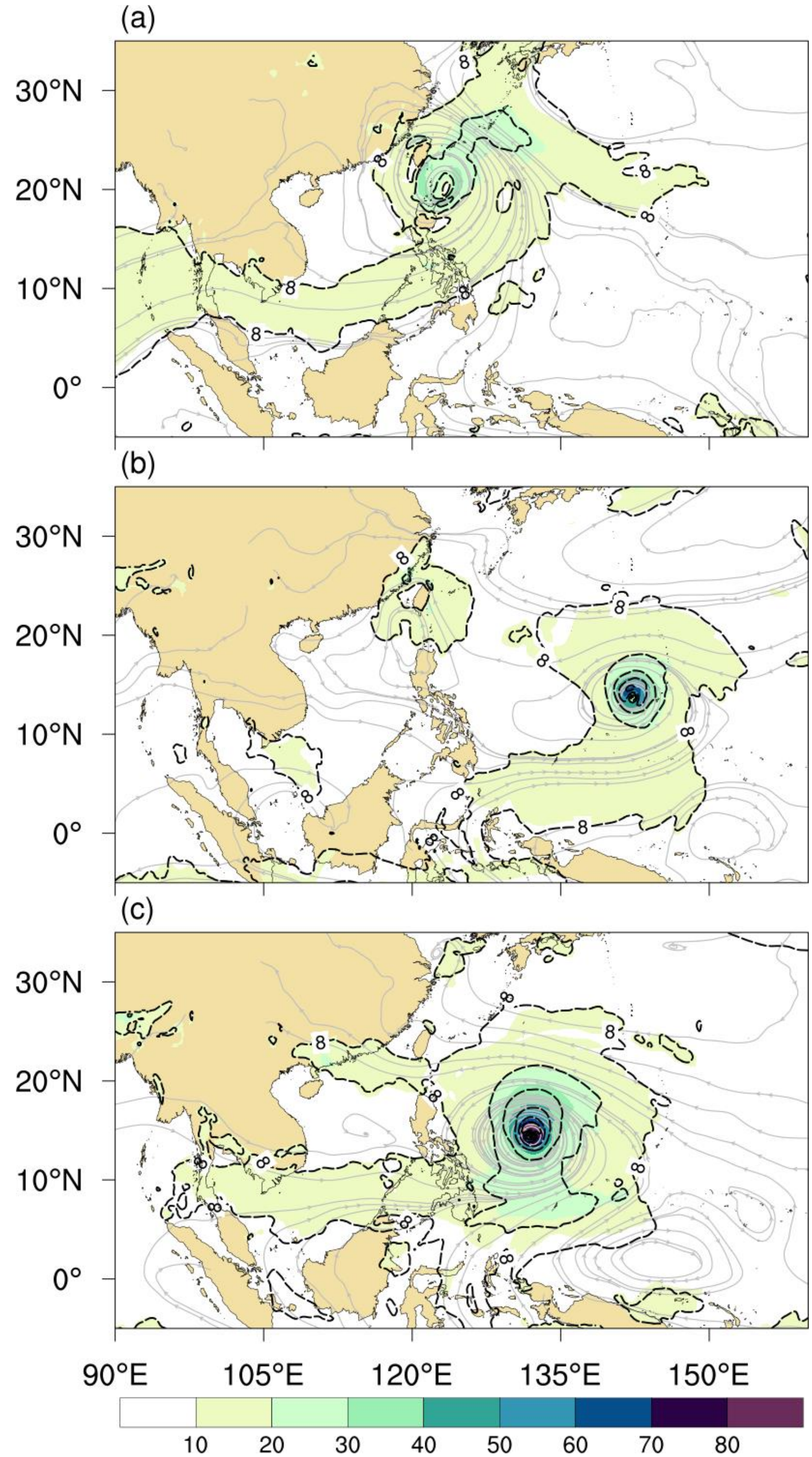

Figure 8. Water vapor fluxes (shadings, unit: kg m^{-1} s^{-1}), isotachs (dashed contours, unit: m s^{-1}), and streamlines at 850 hPa (unit: m s^{-1}) at (**a**) 10 UTC 21 August 2017 (Hato), (**b**) 20 UTC 10 September 2018 (Mangkhut) and (**c**) 21 UTC 12 September 2018 (Mangkhut).

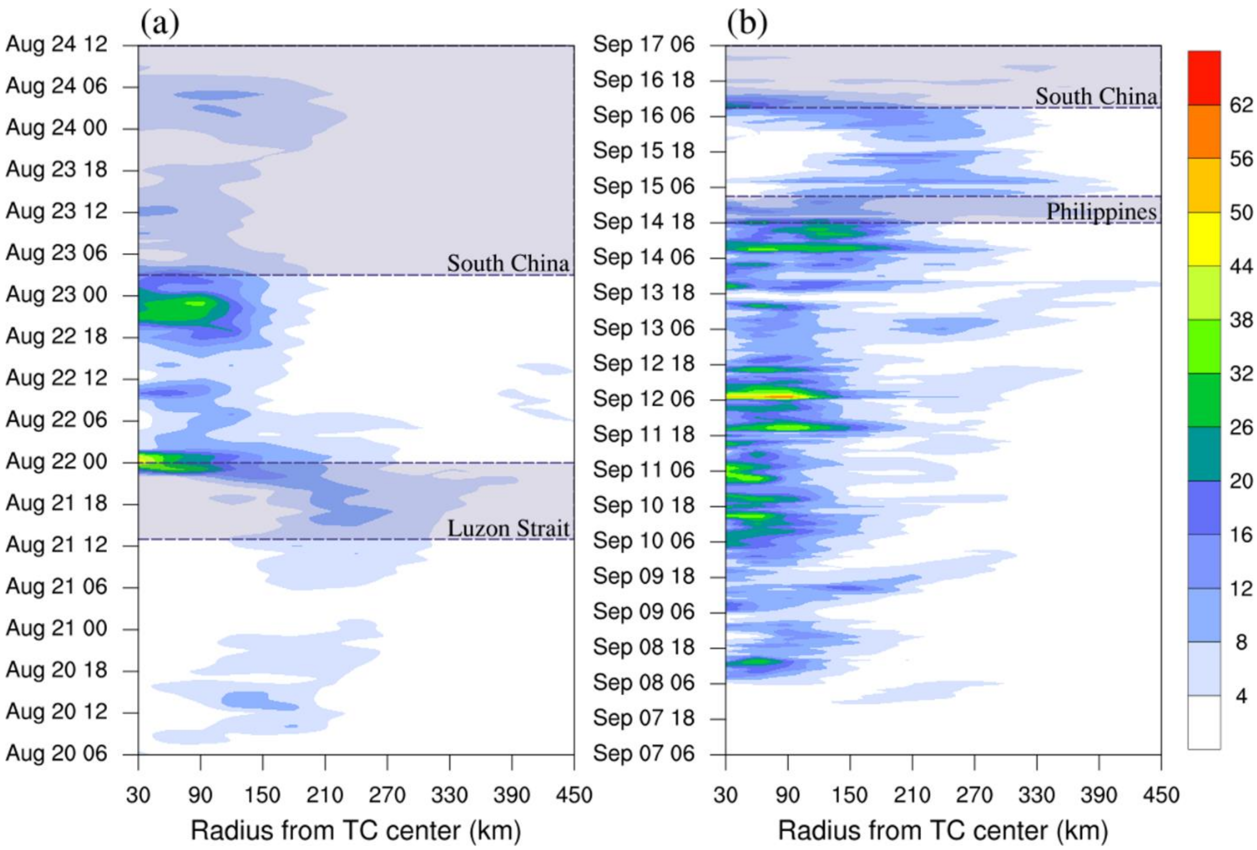

Figure 9. Radius-time Hovmöller diagrams of the azimuthal averages of precipitation rate (unit: mm h^{-1}) at each 60-km ring from the TC centers of (**a**) Hato and (**b**) Mangkhut. The half-transparent strips in light blue denote the time periods that the storms tracked across the specified regions.

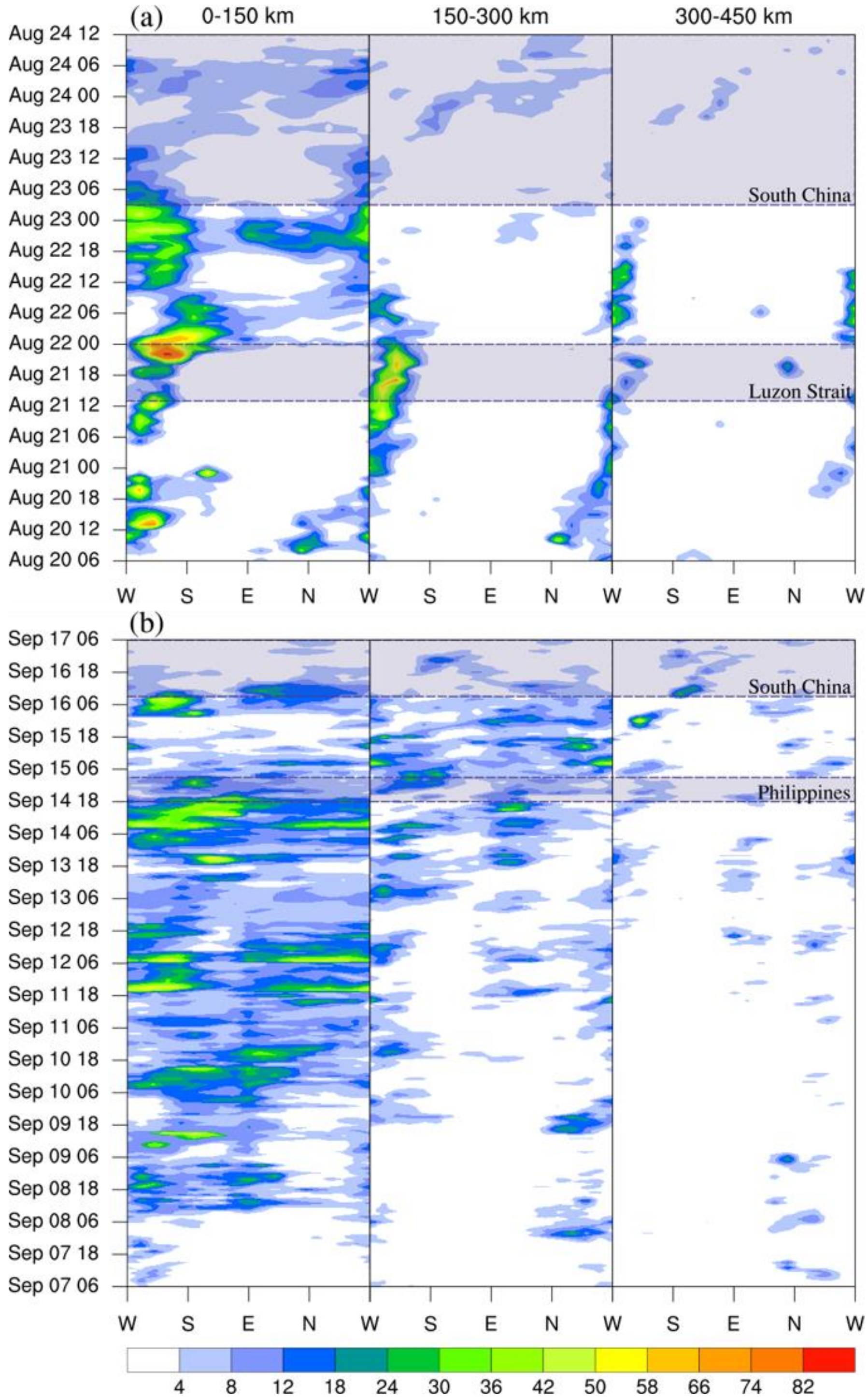

Figure 10. Radius-azimuth Hovmöller diagrams of the averages of precipitation rate (unit: mm h^{-1}) at each 20° azimuth within a radius of (left column) 0–150, (middle column) 150–300 and (right column) 300–450 km from the TC centers of (**a**) Hato and (**b**) Mangkhut. The half-transparent strips in light blue denote the time periods that the storms tracked across the specified regions.

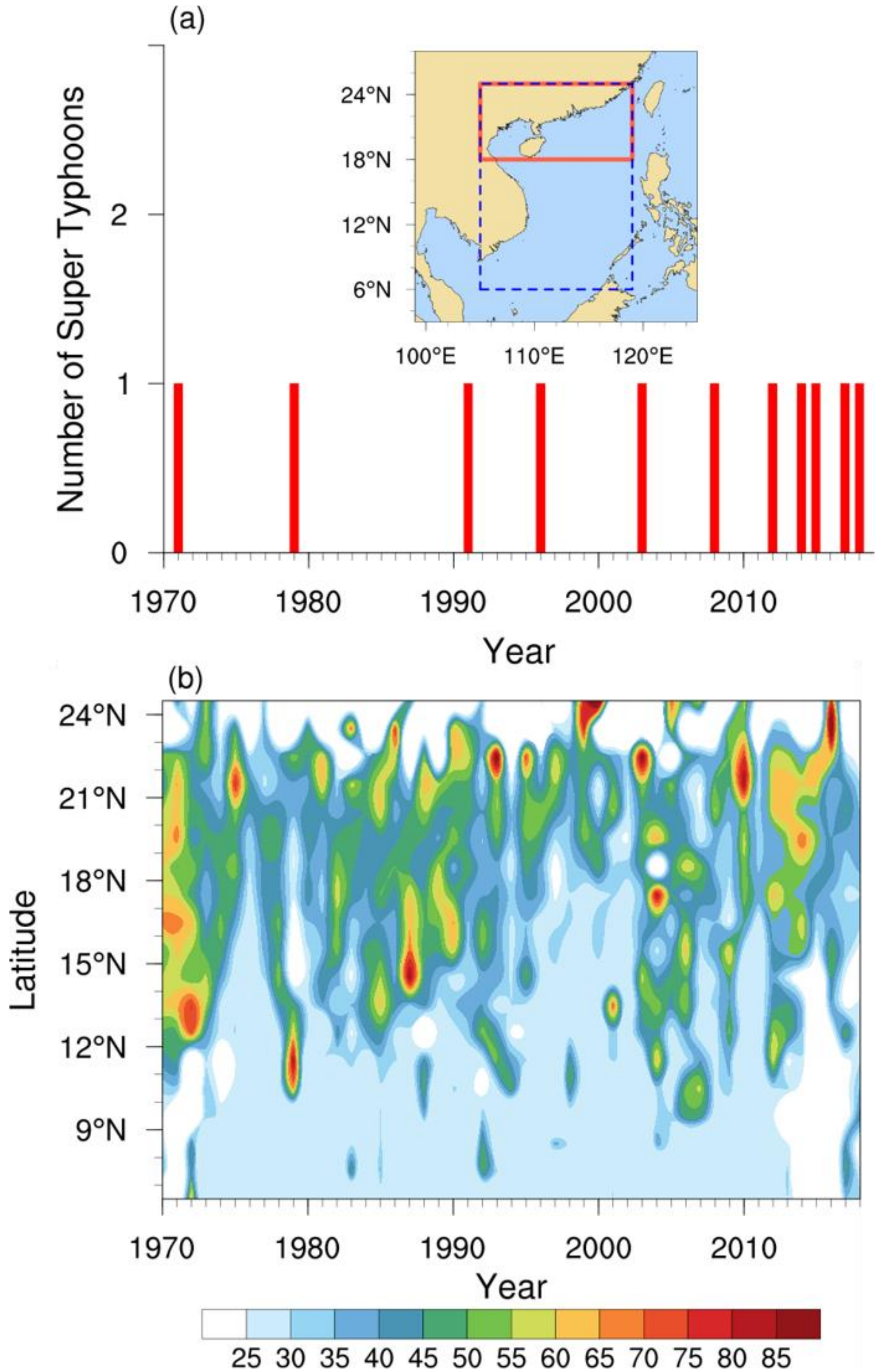

Figure 11. (**a**) Time series of annual number of landfalling Super Typhoons over South China, where the region of South China is denoted by the red solid box on the map. (**b**) Time series of annual average of TC intensity in South China Sea as a function of latitude, where the region of South China Sea is denoted by the blue dashed box on the map in (**a**).